



HAL
open science

Predicting the flowability of alumina powder during batch grinding through the establishment of a grinding kinetic model

Martin Giraud, Stéphane Vaudez, Cendrine Gatumel, Jeremy Nos, Thierry Gervais, Guillaume Bernard-Granger, Henri Berthiaux

► To cite this version:

Martin Giraud, Stéphane Vaudez, Cendrine Gatumel, Jeremy Nos, Thierry Gervais, et al.. Predicting the flowability of alumina powder during batch grinding through the establishment of a grinding kinetic model. *Advanced Powder Technology*, 2021, 32 (9), pp.3207-3219. 10.1016/j.appt.2021.07.006 . hal-03306832

HAL Id: hal-03306832

<https://imt-mines-albi.hal.science/hal-03306832>

Submitted on 16 Oct 2023

HAL is a multi-disciplinary open access archive for the deposit and dissemination of scientific research documents, whether they are published or not. The documents may come from teaching and research institutions in France or abroad, or from public or private research centers.

L'archive ouverte pluridisciplinaire **HAL**, est destinée au dépôt et à la diffusion de documents scientifiques de niveau recherche, publiés ou non, émanant des établissements d'enseignement et de recherche français ou étrangers, des laboratoires publics ou privés.



Distributed under a Creative Commons Attribution - NonCommercial 4.0 International License

Title:

Predicting the flowability of alumina powder during batch grinding through the establishment of a grinding kinetics model

Authors:

Martin GIRAUD^{a,b}, Stéphane VAUDEZ^b, Cendrine GATUMEL^a, Jeremy NOS^c, Thierry GERVAIS^d, Guillaume BERNARD-GRANGER^b, Henri BERTHIAUX^a

^a Laboratoire RAPSODEE, UMR CNRS 5302, IMT Mines Albi, Campus Jarlard, 81013 Albi Cedex 09, France

^b CEA, DEN, DMRC, Université de Montpellier, Marcoule, France

^c Orano, 125 avenue de Paris, 92320 Châtillon, France

^d Orano Melox, Les Tourettes, D138A, 30200 Chusclan, France

Corresponding author:

Martin GIRAUD^{a,b} – martin.giraud14@gmail.com

Abstract:

Grinding is one of the main unit operation in industrial processes handling powders. The particle size reduction that takes place during grinding tests, usually results in a significant change in the flow behavior of the ground powder. Up to now, a model predicting the evolution of powder flowability with grinding time, according to the operating conditions is still missing. In this paper, a methodology combining a grinding kinetic model and a flowability model involving the population-dependent granular Bond number is developed. The methodology has been applied to an alumina powder, ground in a batch ball mill. The flow function coefficient of the ground samples is measured after various grinding times in a powder shear tester. The comparison between model predictions and experimental data shows that this method allows an accurate prediction of the powder flow behavior over the first sixteen minutes of grinding.

Keywords:

powder rheology – grinding kinetics – population balance model – granular Bond number

Nomenclature:

Notation	Parameter	Usual units
A	Intermediate matrix [$A = (B-I) S$]	s^{-1}
B	Breakage matrix	-
b_{ij}	Breakage parameter	-
B_{ij}	Cumulative breakage parameter	-
Bo_g	(population-dependent) Granular Bond number	-
D_0	Cut-off distance	nm
d_{asp}	Surface asperity diameter	nm
d_i	Particle diameter	μm
D_s	Sauter mean diameter	μm
E_D	Diagonal matrix of components $\exp(-S_i t)$	-
ff_c	Flow function coefficient	-
F_{IP}	Interparticle attractive forces	N
g	Gravity acceleration	$m.s^{-2}$
H_A	Hamaker constant	$10^{-19} J$
J	Filling ratio	-
$K_i^{[k]}$	k^{th} Kapur coefficient	s^{-k}
n	Number of size classes	-
P	Passage matrix	-
q	Specific electrostatic charge	$\mu C.kg^{-1}$
R_i	Cumulative mass fraction oversize class i	-
rms	Root mean square	nm
S	Selection matrix	s^{-1}
S_i	Selection parameter	s^{-1}
t	Grinding time	s
U	Powder level	-
V	Intermediate matrix [$V = P.E_D.P^{-1}$]	-
V_i	Volume of the element i	L
W	Particle size distribution vector	-
w_i	Mass fraction of class i	-
W_p	Particle weight	N
Z	Intermediate vector [$Z = P^{-1}.W$]	-
z_0	Interparticle distance	nm
α	Model parameter	-
α_1	Model parameter	-
α_2	Model parameter	-
β	Model parameter	-
ε_g	Pebbles bed porosity	-
ϵ	Total squared error	-
γ_s^d	Dispersive surface energy	$mN.m^{-1}$
μ_D	Intermediate vector	-
ρ_s	Particle true density	$g.cm^{-3}$

Abbreviations:

AFM: Atomic Force Microscopy

DVS: Dynamic Vapor Sorption

PGB: Population-dependent Granular Bond number

1. Introduction

In many industrial processes dealing with particulate media, grinding operations are commonly used in order to reduce the particle size or increase their specific surface area (Austin and Rogers, 1985). Such industrial processes range from heavy industrial plants such as in mineral processing or cement manufacturing, to smaller capacity plants such as for pharmaceutical, ceramic or pigment preparations (Prasher, 1987). However, by decreasing the particle size, the grinding operation is likely to decrease the flowability of the powder bed, making its handling more difficult, if not impossible. This may result in process slow-down or equipment damaging. As highlighted by Schulze, even for simple equipment such as intermediate storage silos, bad dimensioning may lead to powder arching and ratholing that often results in irregular discharge or even complete blockage (Schulze, 2007). Therefore, the flow behavior of the granular materials handled in a given process is a critical parameter that needs to be taken into account while designing mixing, conveying or storage equipment for example.

As reported in previous investigations, the flowability of a given powder depends on the predominance of the interparticle forces (Castellanos, 2005; Liu et al., 2008). These forces, acting at a microscopic scale, are expected to become greater than the particle weight as their size decreases. Such postulate has been confirmed by many experimental investigations focusing on the influence of the particles size and shape on the bulk powder flowability (Fu et al., 2012; Mellmann et al., 2013), this will be discussed further in section 2.1. Thus, the degradation of the powder flowability appears to be almost inevitable in any grinding process.

This means that the grinding parameters, which have a great influence on the ground powder flowability, may affect the processability of the powder through all the following process steps. Up to our knowledge, most grinding kinetic models developed in the literature are focusing on the evolution of the particle size, which is the main variable of interest in the grinding operation. However, the evolution of the ground powder flow behavior according to the grinding time has never been investigated so far; although it appears that it is one of the most critical parameters governing its processability through various operations. Thus, the aim of this paper is to suggest a methodology for predicting the flowability of powders obtained after a given grinding time. Such a method would be of significant industrial interest since it could guide the manufacturers for:

- predicting the expected variations in powder flow according to the grinding time,
- dimensioning the conveyers, silos, mixers that may handle the ground powder accordingly with the grinding time needed,
- defining the optimal grinding conditions that lead to a sufficient particle size without decreasing to much the powder processability.

This work provides a substantial amount of analyzed data in order to reflect as much as possible the empirical observations that can be made in an actual process. The methodology suggested in this paper is described in detail so that it can be reproduced in other conditions.

At this point, it is important to note that we do not infer that the powder's flowability has a direct effect on the grinding mechanisms in the ball mill process. However, its flowability after grinding affects its manufacturability for draining, transport or storage steps that may be present after the milling operation. Thus, the aim of this paper is to assess how the ball mill

process has an influence on the flowability of the ground powder, obtained after grinding rather than during the operation itself.

After discussing the effect of particle size on the overall powder's flowability in section 2.1, the grinding theory will be developed in section 2.2 and 2.3. Then, the equipment, materials and methods employed for the acquisition and the exploitation of the experimental data in section 3. Afterwards, the results of batch laboratory grinding tests corresponding to various durations will be reported for an alumina powder in order to establish the model by comparing the predicted results to experimental data.

2. Theoretical background

2.1. Link between the flowability of a given powder and its particle size distribution

The link between the macroscopic flowability of a given powder and its particle size distribution has been recently developed through the population-dependent granular Bond number (PGB) (Bernard-Granger et al., 2019; Capece et al., 2015). This dimensionless number represents the force balance at the individual particles level. It is defined as the ratio between the interparticle forces and the particle's weight as described in equation (1). This granular Bond number is not expected to represent the powder behavior in a dynamic motion. However, it can be used to assess the ability of the powder to overcome the cohesive forces in a quasi-static regime in order to start flowing. In practice, such a force balance between cohesive and gravitational forces may be of great interest for dimensioning silos, conveyer strips or for defining a draining protocol for a given equipment, such as a powder mixer or a mill.

$$Bo_g = \frac{F_{IP}}{W_p} \quad (1)$$

where W_p is the weight of a given particle and F_{IP} represents the sum of all the interparticle forces contributions. These attractive interparticle forces may be capillary, electrostatic and Van der Waals forces which are responsible for the cohesion of the powders (Seville et al., 2000a).

One of the main advantages of the PGB is that it takes into account the whole particle size distribution while most other models developed in the literature use mean diameters such as the Sauter mean diameter. The PGB of a polydispersed powder can be calculated from equation (2), by taking the weighted harmonic mean of all the potential individual granular Bond numbers, $Bo_{g,ij}$ between the particles belonging to each size classes, indexed from 1 to n (Giraud et al., 2020a).

$$Bo_G = \left(\sum_{i=1}^n \sum_{j=1}^n \frac{z_i \cdot z_j}{Bo_{g,ij}} \right)^{-1} \quad (2)$$

where z_i and z_j corresponds to the surface fraction of the particles belonging to the size classes of index i and j .

It was shown, both theoretically and experimentally, that the PGB correlates well with the powder flow behavior investigated by shear tests (Castellanos, 2005). In particular, Capece found a power law correlation, represented by equation (3), between the macroscopic flow

behavior of a given powder and the microscopic properties of the involved particles, represented by their PGB.

$$ff_c = \alpha \times Bo_G^{-\beta} \quad (3)$$

where α and β are adjustable model parameters and ff_c is the flow function coefficient of the powder, measured by shear testing as will be described in section 3. Such a correlation has then been verified experimentally, focusing on various raw ceramic powders (Bernard-Granger et al., 2019) and pharmaceutical powders as well (Capece et al., 2016). A physical significance has also been suggested for the model empirical parameters α and β based on the Rupmf's theoretical equation (Giraud et al., 2020a). Finally, it has been shown that this correlation is also suitable to predict the flowability of ground powders knowing their particle size distribution (Giraud et al., 2020b). In this last investigation, the correlation represented by equation (4) was found to describe well the behavior of alumina and zirconia powders co-ground in a batch ball mill for various grinding times.

$$ff_c = 179.6 \times Bo_G^{-0.54} \quad (4)$$

This equation (4) shows that if the evolution of the PGB with grinding time was known, it would allow a prediction of the ground powder flowability. This can be achieved with a population balance model which is described in the following sections.

2.2. Population balance in batch grinding and matrix analysis

Since the breakage behavior of a given particle depends on its size, it is common to use the particle size distribution whose size classes are discretized, following geometric screen intervals, indexed from 1 (largest particles) to n (finest ones) (Prasher, 1987). The total amount of size classes, n , mainly depends on the particle size measurement method and on the spread of the distribution. Then, the evolution of the particle size during batch grinding tests can be simulated by resolving the population balance equation for each size class (Austin, 1971). For a given size interval, the population balance can be represented thanks to a kinetic model involving the rate of breakage of the particles and the overall size of the fragmented particles. This is achieved by defining two functions which are usually discretized in the same way as the particle size distribution: the selection function S_i , and the breakage function, b_{ij} (Reid, 1965). The selection function, S_i , can be interpreted as the specific breakage rate associated to the size class i . It represents the mass fraction of the particles of class i that are reduced in size per unit of time or per breakage event. The breakage function, b_{ij} , accounts for the mass fraction of particles belonging to class j that are found in class i ($i < j$) after a breakage event. It can also be understood as the distribution of the fragments obtained after breaking a particle of class j . As a first approach, the selection and breakage function are considered stationary, meaning that they do not depend on the grinding time (Austin, 1971). The evolution of the mass fraction, w_i , of each size class can then be expressed in terms of the selection and breakage functions through the differential equation system (5) (Austin and Bagga, 1981).

$$\frac{dw_i(t)}{dt} = -S_i w_i(t) + \sum_{j=1}^i b_{i,j} S_j w_j(t) \quad (5)$$

In equation (5), the variation of the population of the class i depends on two main terms: a first negative one, accounting for the particles that are broken and leave the class i for higher class numbers, and a second positive one, accounting for the particles coming from smaller class numbers to join the class i particles. A standard method employed to solve such a system is to express it by means of matrices (Berthiaux et al., 1996) as shown in equation (6), where the breakage and selection functions are still considered stationary.

$$\frac{dW(t)}{dt} = AW(t) \text{ with } A = (B - I)S \quad (6)$$

where W is the particle size distribution vector, S is an $n \times n$ diagonal matrix containing the elements S_i of the selection function, B is an $n \times n$ lower triangular matrix containing the b_{ij} elements of the breakage function and I is the $n \times n$ identity matrix.

The first-order linear differential system represented by equation (6) can be solved by diagonalization of the matrix A , a lower triangular matrix whose diagonal elements are the $-S_i$ terms. This means that there is a passage matrix P , constituted of the eigenvectors of matrix A , such that:

$$A = -PSP^{-1} \quad (7)$$

Then, equation (6) transforms as follows:

$$\frac{dW(t)}{dt} = -PSP^{-1}W(t) \quad (8)$$

The equation (8) can be expressed in the form of equation (9) by introducing the substitution vector $Z = P^{-1}W$, noting that P and P^{-1} are not a function of time:

$$\frac{dZ(t)}{dt} = -SZ(t) \quad (9)$$

The equation (9) can be easily integrated, giving:

$$Z(t) = E_D(t)\mu_v \quad (10)$$

where μ_v is a column vector containing the integration constants and E_D is an $n \times n$ diagonal matrix containing the $\exp(-S_it)$ elements.

Finally, noting in equation (10) that $Z(0) = \mu_v$, and substituting Z by $P^{-1}W$, the particle size distribution vector can be computed for any given time t , as long as the initial particle size distribution $W(0)$ is known:

$$W(t) = V(t) \cdot W(0) \text{ with } V(t) = PE_D(t)P^{-1} \quad (11)$$

2.3. Determination of the selection and breakage parameter from Kapur's approximation

In most cases, the selection and breakage parameters are estimated from an empirical approach involving mono-size grindings (Gupta, 2017; Petrakis et al., 2017). Nevertheless, this method is only suitable for a few amount of size classes, typically two or three, and when the particles are large enough (greater than around 50 μm in diameter) to allow separation of the size classes by sieving (Berthiaux et al., 1996). Considering that the precision of the PGB,

as defined in equation (2), increases with the number of size classes, these experimental methods cannot be relevant in our case. For larger number of size classes, some numerical and mathematical methods have been developed (Berthiaux and Dodds, 1997), providing an approximation of the breakage and selection parameters. In this study, we will estimate these two parameters from a method based on Kapur's approximation (Kapur, 1971).

First, we have to express the population balance, represented by equation (5), in terms of the cumulative oversize mass fraction $R_i(t) = \sum_{j=1}^i w_j(t)$:

$$\frac{dR_i(t)}{dt} = -S_i R_i(t) + \sum_{j=1}^{i-1} (S_{j+1} B_{i,j+1} - S_j B_{i,j}) R_j(t) \quad (12)$$

where $B_{i,j} = \sum_{k=j+1}^n b_{k,j}$ is the cumulative breakage function. Kapur's solution (Kapur, 1971) consists in a second order series development, which can be extended to order p , as shown in equation (13).

$$\ln \frac{R_i(t)}{R_i(0)} = \sum_{k=1}^p K_i^{[k]} \frac{t^k}{k!} \quad (13)$$

Berthiaux carried out batch bead mill tests for hydrargillite and carbon suspensions and showed that this approximation even fits the experimental data for the first order ($p = 1$) during the first 15 minutes of grinding, leading to the approximate equation (14) (Berthiaux et al., 1996). The same author also showed that this approximation seems to be consistent with the experimental data obtained by grinding hydrargillite in a jet mill over the first minutes of grinding (Berthiaux and Dodds, 1999).

$$\ln \frac{R_i(t)}{R_i(0)} \approx K_i^{[1]} t \quad (14)$$

where the $K_i^{[1]}$ coefficients can easily be found from experimental data that are acquired during the initial period of grinding through log-linear representation. It is worth noting that for longer grinding times the approximation may become no longer relevant, while the selection and breakage parameters found are still valid.

Then, the selection and breakage functions can be deduced from a mathematical treatment derived directly from equation (14) (Berthiaux et al., 1996).

$$S_i = -K_i^{[1]} \quad \text{and} \quad b_{i,j} = \frac{K_{i-1}^{[1]} - K_i^{[1]}}{K_j^{[1]}} \quad (b_{i \leq j} = 0) \quad (15)$$

As long as the approximation equation fits the particle size distributions data set (14), this method allows an easier determination of the breakage and selection functions, whatever the number of size classes considered. As a result, S and B matrices can be built up and equation (11) can be employed to compute the model and predict the particle size distribution for grinding times longer than those considered in the approximation, since B and S are supposed to be stationary.

3. Materials and methods

3.1. Powder

An alumina (Al₂O₃) GE15 powder, from Baikowski® (Poisy, France) was used for this study. It was chosen for its medium flowability and its specific particle size distribution, as compared to other ceramic oxide powders investigated previously (Giraud et al., 2020a).

3.2. Preparations in a ball mill

The ball mill is a 1 L cylindrical (116x106mm) stainless steel vessel, filled with 500 cylindrical 8x8 mm steel pebbles, which are used as grinding media. A representation of the experimental setup is provided in Figure 1. The powder is introduced in the vessel and the supporting rolls induce the rotation of the cylindrical vessel horizontally around its longitudinal axis, as shown in Figure 1. The rotation of the vessel is controlled by a potentiometer graduated from 0 to 100 and the rotational speed can be measured by a tachometer DT-2236® (Luron electronic, Taipei, Taiwan). When the vessel is rotating, the powder in contact with the pebbles is fragmented through various mechanisms:

- compaction under the weight of the pebble bed,
- shearing due to friction forces between the moving pebbles,
- impact when the pebbles are ejected from the pebble bed and collapse on the powder (Arai, 1996).

However, in practice, according to the size of the alumina particles, the powder might be mostly ground because of shearing fragmentation mechanisms (Arai, 1996).

Although wet grinding is generally preferred because of the lower grinding energy needed, dry grinding was performed in this investigation. Such operation is still used in various industrial processes where the products may be damaged or dissolved in water or other liquids. The amount of pebbles and powder filled into the vessel is adjusted in order to get a constant filling ratio of $J = 0.3$ (see equation (16)) and a powder level of $U = 1.00$ (see equation (17)). This corresponds to a number of 500 pellets and a mass of 35.90 g of alumina powder introduced into the vessel. Such filling conditions are commonly employed as they seem to correspond to optimal operating conditions for a ball mill (Prasher, 1987; Shoji et al., 1982).

$$J = \frac{V_{pebbles}}{V_{vessel}} \quad (16)$$

$$U = \frac{V_{powder}}{\varepsilon_g \cdot V_{pebbles}} = \frac{V_{powder}}{\varepsilon_g \cdot J \cdot V_{vessel}} \quad (17)$$

where V_{vessel} is the total volume of the vessel (here 1 L), V_{powder} is the apparent volume of the powder bed before grinding when poured into the vessel, $V_{pebbles}$ is the apparent volume of the pebbles bed and $\varepsilon_g = 0.33$ is the porosity of the pebbles bed when the vessel is not rotating. The value of ε_g was determined experimentally by measuring the volume of water needed to fill the porosities between the pebbles within the vessel.

The vessel is rotating horizontally around its radial axis at 25 rpm, which corresponds to a Froude number (ratio between the centrifugal and gravitational forces at the edge of the vessel) of 0.04. This rotational speed was defined in order to ensure a cascade motion regime

of the pebbles into the vessel, which is adequate for grinding the powders (Mellmann, 2001; Rumpf, 2012). The cataracting regime may also be suitable for grinding the powders but there is still a risk of deteriorating the pebbles and the vessel due to the repeated impacts between the falling pebbles and the vessel's walls.

Various grinding tests were carried out with exactly the same conditions described above but for different grinding times. The ball mill was stopped successively after 0.4, 1, 2, 4, 6 and 8 minutes of grinding. Finally, another grinding test of 16 minutes long was carried out in order to check the consistency of the predictions after a longer grinding period.

3.3. Characterization methods

The following characterizations were carried out on the alumina powder before and after grinding, in order to calculate the PGB values. For this study, we assumed that the true density, the Hamaker constants and the surface asperity diameters remained the same before and after grinding. These assumptions are discussed respectively in sections 3.3.3, 3.3.4 and 3.3.5.

3.3.1. Powder flowability

The flowability of the powder samples was assessed by shear testing with a FT4® (Freeman, Tewkesbury, UK) powder rheometer. Tests were carried out in a 10 mL cylindrical glass cell under a normal pre-consolidation stress of 9 kPa, according to the Jenike standard procedure (EFCE, 1989). After pre-conditioning steps and successive tests under various consolidation stresses (3, 4, 5, 6 and 7 kPa), the yield locus and the Mohr circles can be plotted according to Mohr's theory. Ultimately, the dimensionless flow function coefficient ff_c can be computed from the Mohr circles (Seville et al., 2012). This index is commonly used to evaluate the flow behavior of powders according to the classification given in Table 1 (Leturia et al., 2014). The flow function coefficient is related to the shear stress needed to overcome the cohesive forces and thus yield the powder bed in a quasi-static regime. This explains why it seems closely related to the granular Bond number, which represents the same thing at a particle scale, as shown in equation (3).

Each measurement was performed at least twice on different powder samples. The ff_c values given in Table 2 correspond to their mean value and the standard deviations are taken as uncertainty intervals. Since capillary forces may also influence the flowability (Seville et al., 2000b) of the powders, all the samples were dried in a stove at 110 °C for 24 hours before any rheological measurement.

3.3.2. Particle size distribution

The volume particle size distribution of the powder samples were measured by LASER diffraction using a Mastersizer 3000® (Malvern, Malvern, UK) device equipped with a Hydro MV® liquid dispersion unit. Dry dispersion measurements were also attempted but the results were not enough robust and stable for exploitation. This is possibly due to a re-agglomeration phenomenon taking place during the conveying step or pneumatic transport through the Venturi of the Malvern® equipment. For each ground powder, five samples were analyzed by taking ten measurements on each sample. The results after different grinding times are given on Figure 2 and the corresponding Sauter mean diameters are reported in the third column of

Table 2 for an incertitude interval corresponding to the standard deviation of the data. As expected, we can observe that the particles become smaller as the grinding time increases.

The surface particle size distribution, involved in the calculation of the PGB, as defined in equation (2), can be deduced from the volume particle size distribution thanks to equation (18).

$$z_i = \frac{w_i}{d_i} \times \left(\sum_{j=1}^n \frac{w_j}{d_j} \right)^{-1} \quad (18)$$

where z_i and w_i correspond respectively to the surface and volume fractions associated to the size class index i .

3.3.3. True density

The true density of the alumina powder was measured with a helium pycnometer AccuPyc II 1340® (Micromeriticsn Mérégnac, France) in a 10 mL cell. Five different powder samples were measured between three and five times each. Each measurement cycle includes 25 purges followed by 25 measurements carried out at 23 °C and 135 kPa. The measured true density of the alumina GE15 powder has been determined as $\rho_s = 4.017 \pm 0.070 \text{ g} \cdot \text{cm}^{-3}$, where the incertitude corresponds to the standard deviation between the samples.

In order to estimate the influence of grinding on the true density of the alumina powder, another sample has been considered in the same conditions after 5 minutes of grinding. Such a ground alumina powder sample exhibits a true density of $\rho_{s,ground} = 4.080 \text{ g} \cdot \text{cm}^{-3}$ which does not represent a significant modification considering that this value is included in the incertitude interval given above for measurement completed on the raw powder. Therefore, we assume that the true density remains constant throughout the grinding process and thus a constant value of $\rho_s = 4.017 \pm 0.070 \text{ g} \cdot \text{cm}^{-3}$ can be considered.

3.3.4. Particle surface energy

The dispersive surface energy of the alumina particles was measured by analyzing the heptane vapor sorption and desorption isotherms acquired with a dynamic vapor sorption (DVS) equipment (SMS, London, UK). The Fowkes model was used to compute the dispersive surface energy γ_s^d from the DVS measurements (Tisserand et al., 2009). The Hamaker constant H_A was then computed using the Frenkel equation (Israelachvili, 2011):

$$H_A = 24\pi D_0^2 \gamma_s^d \quad (19)$$

where $D_0 \approx 0.165 \text{ nm}$ is a cut off distance.

The measurements were carried out on two different powder samples, driving to an average value of $H_A = (1.57 \pm 0.03) \times 10^{-19} \text{ J}$, the incertitude corresponding to the standard deviation between both measurements.

Like for the true density, the Hamaker constant of the alumina powder was measured following exactly the same protocol after 5 minutes of grinding. The result shows that the obtained value after grinding is $H_{A,ground} = 1.61 \times 10^{-19} \text{ J}$, which is not significantly different to the initial value, moreover when considering the incertitude intervals. We

therefore assume that the Hamaker constant does not change with the grinding time and the same value of $H_A = (1.57 \pm 0.03) \times 10^{-19} J$ can be considered.

3.3.5. Particle surface asperities

Among all the particle characteristics needed to estimate the interparticle forces magnitude, the surface asperity diameter is the most difficult one to measure experimentally. However, the approximate value of $d_{asp} = 200 nm$ can be considered reasonably since previous studies showed that it reflects well the size of natural roughness at a given particle surfaces (Beach et al., 2002). Complementary atomic force microscopy (AFM) measurements were carried out on the powder investigated, in contact mode with a confocal Raman microscope alpha300 R (WITec®, Ulm, Germany), resulting in an average root mean square, *rms*, value of $rms = 195.3 \pm 17.9 nm$, which tends to confirm the usual approximation of $200 nm$. However, considering that only three particles were analyzed, we will stick with an approximate value of $d_{asp} = 200 nm$ for the interparticle forces calculations.

Considering the difficulty of such measurements, we assume that the surface asperity diameter remains constant throughout a grinding test. However, such an assumption could not be checked experimentally and might be wrong in practice. Indeed, the surface asperity diameter may either decrease or increase, due to smoothing of the particles or small particles inclusions during the grinding operation. This is to keep in mind while exploiting the results.

3.3.6. Electrostatic charge

A tribo-electrification technique was employed in order to estimate the specific electrostatic charge developed by the alumina powder. A few grams of powder was incorporated into a cylindrical stainless steel vessel, similar to the ball mill vessel, isolated from the ground and rotating at 92 rpm. The powder samples are then introduced in a Faraday cage after a given time spent in the rotating cylinder, in order to measure the total charge acquired thanks to an electrometer. The initial specific charge of the alumina powder was measured to be $q = + 1.6 \mu C \cdot kg^{-1}$ and remains quite stable up to 15 minutes in the rotating vessel. From this value, it can be shown that the corresponding electrostatic force is considerably smaller than Van der Waals forces, using common electrostatic and Van der Waals force models (Bernard-Granger et al., 2019). As an example, for a $15 \mu m$ particle diameter, close to the measured Sauter mean diameter of the raw alumina powder investigated, the magnitude of the electrostatic force is $10^{-19} N$ while in the same time the Van der Waals forces contribution is around $10^{-4} N$.

3.4. Interparticle forces

In this paper, we assume that the Van der Waals forces are the only relevant interparticle forces and the other force contributions are neglected. Indeed, as explained previously in section 3.3.1, all the powder samples are dried in a stove before any rheological measurement, removing all the residual humidity which is likely to generate capillary forces within the powder. Moreover, as shown in the previous section 3.3.6 the electrostatic forces are clearly negligible when compared to the magnitude of the Van der Waals ones.

Thus, the granular Bond number between two particles of diameters d_i and d_j of the same given powder in close contact can be expressed from equation (20), where the Van der Waals forces are estimated from the modified Rumpf equation (Chen et al., 2008). In this equation,

we assume that two particles of the same mono-constituent powder would share the same Hamaker constant H_A , true density ρ_s and surface asperity diameter d_{asp} . Thus, the values corresponding to the alumina powder investigated, obtained in sections 3.3.3, 3.3.4 and 3.3.5 can be employed to calculate the PGB after each grinding time.

$$Bo_{g,ij} = \frac{H_A}{2\pi\rho_s g z_0^2} \times \frac{\hat{d}}{\sqrt{d_i^3 d_j^3}} \left(\frac{1}{2 \left(1 + \frac{d_{asp}}{2z_0}\right)^2} + \frac{3d_{asp}}{d_{asp} + \hat{d}} \right) \quad (20)$$

where g is the gravity acceleration, $z_0 = 0.4 \text{ nm}$ is the typical interparticle distance in close contact (Molerus, 1982) and $\hat{d} = 2 \frac{d_i d_j}{d_i + d_j}$ is the harmonic mean of diameters d_i and d_j .

Finally, the PGB can be computed by calculating all the individual granular Bond numbers, $Bo_{g,ij}$, between particles of size classes i and j and further combining them with equation (2), knowing the surface particle size distribution. The PGB values obtained after each grinding time are summarized in Table 2.

4. Results and discussion

The methodology employed in order to predict the flowability of the ground powders according to the grinding time is represented schematically on Figure 3. The first step (kinetic model) consists in simulating the evolution of the particle size distribution during the grinding tests from the population balance kinetic model described in section 2. Then, the second step (rheological model) consists in calculating the PGB corresponding to the particle distribution predicted in the first step. Finally, the flow function coefficient of the ground powder is calculated after any grinding time from the power law model, represented by equation (3). It can be noted that both kinetic and rheological models are independent and may be applied separately. However, both models are needed in order to predict the evolution of the powder's flowability according to the grinding time. The aim of this paper is to link both models in order to be able to anticipate the variations in the powder's flowability after various grinding durations.

4.1. Size classes number for the particle size distribution

The total amount of size classes, n , can be interpreted as the resolution of a given particle size distribution. For a given maximal and minimal particle diameters, n defines the spread of the size classes. In our case, the Malvern® equipment gives the volume particle size distribution over 100 size classes ranging from 10 nm to 3.5 mm with a common ratio of 1.136, meaning that each class center corresponds to 1.136 times the center of the lower class. However, the particle size distributions obtained by such a method have to be adjusted before calculating the selection and breakage parameters. Indeed, the number of size classes selected appears to be a critical parameter of the model for the various reasons listed below.

First, a small number of size classes leads obviously to less information implemented into the population balance model, which results in a loss of precision for the prediction of the grinding kinetics. Moreover, it should be highlighted that the particle size distribution is the main input for the calculation of the PGB, meaning that its precision depends on the resolution of the particle size distribution which is directly related to n . In particular, the PGB

appears to be highly sensitive to the population of fine particles (Giraud et al., 2020a), this means that a high precision is required for the particle size distribution, especially for the fraction of fine particles, those diameter are under 10 μm . Second, a high number of size classes may result in a very low amount of particles in some classes. These size classes are then too selective and thus not consistent, leading to incoherence in the definition of the selection function from Kapur's approximation. Finally, the logarithmic form of equation (13) requires avoiding empty classes within the first size classes.

To summarize, the number of size classes, n , should be high enough as it represents the resolution of the model input, but not too high in order to avoid empty or irrelevant classes. Accordingly, the particle size distributions provided by the Malvern® equipment have been manipulated in order to meet these requirements. Firstly, no particle was measured below 0.872 μm whatever the grinding time, meaning that all the classes defined under this limit are empty classes that need to be removed. The measured maximal particle size varied between 454 μm , for the raw alumina powder, and 111 μm , for the alumina powder ground for 8 minutes. Since empty classes must be avoided within the first classes, all the classes defined above 454 μm were removed and the thirteenth classes from 111 to 454 μm were merged together. This leaves exactly 38 relevant size classes ranging from 0.872 to 454 μm . It should be noted that grouping thirteen classes at the beginning of the distribution won't affect significantly the PGB since it mostly depends on the population of fine particles, represented by the last classes of the distribution, as shown in previous investigations (Giraud et al., 2020a). Then selection and breakage parameters can be determined with $n = 38$, which corresponds to the highest possible resolution for this investigation.

Up to our knowledge, the effect of having too many size classes (or a resolution too high) on the population balance model has not been investigated in depth in the literature since this model is often used for particle size distributions obtained by seizing the powder, which rarely involves more than ten size classes. In this paper, the model is applied to particles size distributions measured by LASER dispersion which gives much smaller size classes. In order to investigate the effect of the particle size distribution's "resolution", another estimation of the selection and breakage parameters have been carried out by taking a smaller amount of size classes. This was achieved by merging the 100 initial classes five by five, removing empty classes and merging the first three classes together, as represented schematically on Figure 4. This brings the total amount of size classes to $n = 8$.

The repartition of the size classes for $n = 38$ and for $n = 8$ is represented schematically on Figure 4. The cumulative mass fraction corresponding to both configurations after 6 minutes of grinding are compared on Figure 5.

Accordingly, the methodology described in sections 2.1 and 2.2 has been applied twice, in order to predict the particle size distributions of the ground alumina powder for different amount of size classes $n = 8$ or $n = 38$.

4.2. Modelling grinding kinetics

The first step for predicting the evolution of the particle size distribution of the alumina powder investigated is to determine the selection, S , and breakage, B , matrices (Gupta, 2017). Since the dimension of the selection and breakage matrices is equal to the number of size classes, the number of parameters to be estimated will depend on whether the particle size

distribution is defined over 38 or 8 classes. Indeed, if $n = 38$, there will be 38 selection parameters (diagonal matrix) and 703 breakage parameters (lower triangular matrix) to be estimated. For $n = 8$, there will be only 8 selection parameters and 28 breakage parameters to be estimated. In order to avoid overloading figures and tables, the results of the next paragraph will focus on the case where the particle size distribution is defined over 8 size classes ($n = 8$). It must be noted that the same procedure was carried out for 38 size classes, leading to similar results.

As introduced in section 2.2, the S_i and b_{ij} parameters can be computed from Kapur's first order approximation represented by equation (14). This approximation suggests that the cumulative oversize fraction of each size class varies exponentially with the grinding time. In order to verify this hypothesis, the logarithm of the cumulative oversize fraction for each class has been plotted as a function of the grinding time on Figure 6 for $n = 8$. It appears that Kapur's approximation is rather good for all of the size classes except for the first one. Concerning the first class, the validity of the model seems to hold until 4 minutes of grinding only. This can be explained by the fact that there is a very small amount of particles remaining in this class after few minutes of grinding. Indeed, the mass fraction corresponding to the first class represents 9.97% before grinding and only 0.52% after 6 minutes of grinding, which may explain why the linear breakage law does not seem to stand for this class after a few minutes of grinding. Thus, the first Kapur coefficient $K_1^{[1]}$ has been calculated by removing the last two points corresponding to grinding times of 6 and 8 minutes on Figure 6. All the coefficients $K_i^{[1]}$ corresponding to each size class when $n = 8$ are summarized in Table 3, along with the total squared error, ϵ_i associated. For information, if all the points were to be considered for the first size class, the corresponding squared error associated to Kapur's approximation would be $\epsilon_1 = 0.7643$ instead the actual error of $\epsilon_1 = 0.0014$ obtained by removing the last two points.

Then, the selection and breakage parameters are computed from equation (15) using the $K_i^{[1]}$ values given in Table 3, the corresponding matrices are then given in equations (21) and (22) respectively.

$$S = \begin{pmatrix} 0.25 & 0 & 0 & 0 & 0 & 0 & 0 & 0 \\ 0 & 0.15 & 0 & 0 & 0 & 0 & 0 & 0 \\ 0 & 0 & 0.07 & 0 & 0 & 0 & 0 & 0 \\ 0 & 0 & 0 & 0.04 & 0 & 0 & 0 & 0 \\ 0 & 0 & 0 & 0 & 0.03 & 0 & 0 & 0 \\ 0 & 0 & 0 & 0 & 0 & 0.01 & 0 & 0 \\ 0 & 0 & 0 & 0 & 0 & 0 & 0 & 0 \\ 0 & 0 & 0 & 0 & 0 & 0 & 0 & 0 \end{pmatrix} \quad (21)$$

And

$$B = \begin{pmatrix} 0 & 0 & 0 & 0 & 0 & 0 & 0 & 0 \\ 0.41 & 0 & 0 & 0 & 0 & 0 & 0 & 0 \\ 0.31 & 0.52 & 0 & 0 & 0 & 0 & 0 & 0 \\ 0.11 & 0.19 & 0.40 & 0 & 0 & 0 & 0 & 0 \\ 0.06 & 0.11 & 0.22 & 0.37 & 0 & 0 & 0 & 0 \\ 0.06 & 0.10 & 0.21 & 0.34 & 0.54 & 0 & 0 & 0 \\ 0.04 & 0.07 & 0.14 & 0.23 & 0.37 & 0.80 & 0 & 0 \\ 0.01 & 0.02 & 0.03 & 0.06 & 0.09 & 0.20 & 1 & 0 \end{pmatrix} \quad (22)$$

The selection parameters, S_i , can be interpreted as kinetic constants, expressed in min^{-1} associated to each size class. For example, the kinetic constant associated to the breakage of the particles belonging to the second class, whose particle diameters ranges from 35.3 to

33.9 μm , is $S_2 = 0.15 \text{ min}^{-1}$. Therefore, the decreasing values of the S_i parameters with the particle size reflects the fact that it is more difficult to grind small particles than large ones. Figure 7 shows the values of the S_i parameters obtained as a function of the particle size d_i , where d_i is taken as the upper diameter of the class i . Only six points are represented since the values of S_7 and S_8 worth zero in equation (21). It appears that the selection parameters evolve with the particle size according to a power law represented by equation (23), as commonly reported in the literature (Austin, 1971), with $\alpha_1 = 0.0050$ and $\alpha_2 = 0.6976$.

$$S_i = \alpha_1 \times \left(\frac{d_i}{d_0}\right)^{\alpha_2} \quad (23)$$

where $d_0 = 1 \mu\text{m}$ is the unit size needed for the dimensional homogenization.

As explained previously, the columns constituting the breakage matrix, B , represent the particle size distribution after grinding one size class only. For example, the second column of the B matrix indicates that 52 % of the particles belonging to the second class (35.3 – 66.9 μm) are going in the third class (18.7 – 35.3 μm) once ground, while only 2 % of them are fragmented into the last class ($\leq 1.45 \mu\text{m}$). For all the size classes, it is interesting to note that most particles that are being ground are going into the two following classes. Such a behavior may suggests that the ball milling process is mainly inducing a de-agglomeration of the powder into blocks that may be pre-existent in the particle's structure, rather than a destructive fragmentation of the particles. The evolution of the cumulative breakage parameters, B_{ij} , is represented as a function of the size ratio (d_i/d_j) on Figure 8. It appears that most of the breakage events lead to a size reduction that does not exceed one tenth of the initial particle size.

Then, the methodology described in section 2.1 is employed in order to solve the population equation given by equation (6). The passage matrix, P , is constituted of the eigenvectors of the invertible matrix $A = (B - I) \times S$, which can be computed numerically with the Matlab® software. The same software is used to get the inverted P^{-1} matrix. Finally, the particle size distribution vector, $W(t)$, can be expressed as a function of the initial particle size distribution of the alumina powder, $W(0)$, and a square matrix, $V(t)$ according to equation (11). Figure 9 shows that the model predictions after six minutes of grinding are in good agreement with the actual particle size distribution measured by LASER diffraction, for $n = 8$.

According to Figure 9, the model predictions seem to be quite close to the experimental particle size distribution measured after six minutes of grinding. The Sauter mean diameter has been calculated for each grinding time from the particle size distributions measured by LASER diffraction and those predicted by the model, with $n = 8$. The results are compared on Figure 10, where the predicted values are very close to the experimental ones. This result confirms that the model allows a good prediction of the particle size distributions for all the grinding times from 0.4 to 8 minutes.

The results obtained by applying the same methodology for a larger number of size classes $n = 38$ are also represented on Figure 10. It appears that in this case, the Sauter mean diameter obtained from the experimental and from the predicted particle size distributions are also very close, showing that the model is also suitable for a larger number of size classes. It can also be noticed that the Sauter mean diameter values are varying depending on the number of size classes considered, even if they are calculated from the same particle size

distribution. This issue will be addressed in the next section 4.3. In order to compare quantitatively the results obtained when the number of size classes varies from 8 to 38, the total squared error between the predicted and measured particle size distributions after 0.4, 1, 2, 4, 6 and 8 minutes of grinding for both configurations are given in Figure 11. It clearly appears that the predictions are more robust when the number of size classes is larger. Indeed, for each grinding time, selecting 38 classes instead of 8 allows to reduce the error between predicted and experimental values by a factor of 3.

This shows that such a grinding model, based on the population balance, is suitable for particle size distributions obtained by LASER dispersion, even though the size classes are substantially finer than those used traditionally by sieving.

4.3. Evolution of the granular Bond number according to the grinding time

As explained in the introduction (section 1), the PGB can be calculated for any given particle size distribution by combining equations (2) and (20), thanks to the properties of the alumina GE15 particles measured in section 3.3. Thus, the particle size distributions predicted in the previous section 4.2 can be employed to predict the evolution of the PGB as a function of the grinding time. Figure 12 shows the evolution of the PGB computed from the measured particle size distributions (shown in Figure 2), as compared to those computed from the grinding kinetic model for a size class number set either to $n = 8$ or $n = 38$. The obtained values are also reported in Table 4. It appears that the predictions made from the particle size distributions defined over 8 size classes only, lead to significant errors in the PGB when compared to experimental results. On the other hand, the calculations made with $n = 38$ lead to predicted PGB that are very similar to the experimental ones. Indeed, the variation between the measured PGB and the model predictions for $n = 38$ are almost included in the uncertainty intervals given in Table 4.

By the way, it is also interesting to observe, on the first line of Table 4, that even the PGB values obtained before grinding the powder, where no kinetic model is needed, are significantly different. The only difference between those values is the number of classes: 50 for Bo_G^{exp} , 38 for $Bo_G^{n=38}$ and 8 for $Bo_G^{n=8}$. This highlights the fact that merging the size classes five by five for the whole distribution leads to completely different Bond number values. On the other hand, grouping only the thirteenth first classes together doesn't affect the computed Bond number that much, as the comparison between Bo_G^{exp} and $Bo_G^{n=38}$ shows. This underlines the fact that the population-dependent granular Bond number is highly affected by the precision of the particles size distribution and depends especially on the fraction of the finest particles, as reported recently (Giraud et al., 2020a). This was also visible on Figure 10 where the Sauter mean diameters appeared to be significantly different depending on the number of size classes considered from the same particle size distribution.

Then, the PGB of the ground powders can be predicted when considering $n = 38$ size classes, as shown in Figure 12. This allows to express the PGB of a given ground powder directly as a function of the initial particle size distribution and the grinding time. Indeed, it is possible to get the mass fraction $w_i(t)$ of the size class i after any grinding time by combining Kapur's approximation, represented by equation (14), with the experimental equation (23) found previously and with equation (15). This results in equation (24).

$$w_i(t) = R_i(0) \times \exp(-\alpha_1 d_i^{\alpha_2} t) - R_{i-1}(0) \times \exp(-\alpha_1 d_{i-1}^{\alpha_2} t) \quad (24)$$

where $R_i(0)$ is the cumulative mass fraction of class i before grinding and α_1 and α_2 have been found experimentally in section 4.2 and are specific to the alumina powder investigated.

The surface fractions $z_i(t)$ can be deduced by converting the mass fraction according to equation (18). Then, the surface fraction predicted from the kinetic model can be directly implemented in the PGB as defined in equation (2), providing a definition of the PGB, $Bo_G(t)$, after a given grinding time, as described in equation (25).

$$Bo_G(t) = \left(\sum_{i=1}^n \sum_{j=1}^n \frac{z_i(t) \cdot z_j(t)}{Bo_{g,ij}} \right)^{-1} \quad (25)$$

It should be noted that equation (25) is valid only if the individual granular Bond number between two particles i and j is considered stationary, meaning that the Hamaker constant, the true density and the asperity diameter are not affected by the grinding process.

4.4. Evolution of the flowability according to the grinding time

Since the evolution of the PGB during grinding has been predicted by a grinding model in section 4.3, the flowability of the ground alumina powder can also be predicted. Indeed, as explained in the introduction (section 1), the PGB is linked to the flow function coefficient according to a power law represented by equation (3). In particular, model coefficients $\alpha = 179.6$ and $\beta = 0.54$ were found to fit the behavior of the same ground alumina GE15 powder as shown in equation (4) (Giraud et al., 2020b). The time-evolution of the flow function coefficient obtained in this investigation (see first column in Table 2) has been plotted on Figure 13 as a function of the corresponding PGB (see last column in Table 2). We can notice in Figure 13 that the experimental data, represented by crosses, are not far from the model predictions made from the previously found equation (4), represented by the grey line on Figure 13. The total squared error associated to the model equation (4) is $\epsilon_{(4)} = 4.16$. However, equation (26), whose coefficients have been adjusted by the least square method, is a better power law fit for the experimental data, with a corresponding total squared error of $\epsilon_{(23)} = 0.16$. This equation is represented by the black line on Figure 13.

$$ff_c(t) = 75.3 \times Bo_G(t)^{-0.43} \quad (26)$$

Finally, the flow function coefficients of the ground powders can be computed from the PGB predicted with the population balance model, thanks to equation (26). The predicted flow function coefficients are represented by the continuous line on Figure 14, where the actual experimental measurements are represented by the crosses. The residuals, corresponding to the differences between the measured and predicted values, are shown on the top right corner of the figure. It appears that the residuals seem to be distributed fairly randomly, although more data would be needed in order to carry out a proper residual analysis. Overall, it appears that the model predictions are in very good agreement with the experimental data. This shows that the evolution of the powder flowability as a function of the grinding time is predictable from the particle properties and from the initial particle size distribution of the raw powder, provided that a grinding kinetic model is known.

In order to check the consistency of the model for longer grinding durations, another grinding test of the same powder has been carried out in the ball mill for 16 minutes, with the same conditions described in section 3.2. The measured flow function coefficient is represented on Figure 14 with the other experimental results. Then, the complete methodology is applied in order to get a prediction of the flow function coefficient of the alumina powder after 16 minutes of grinding. First, the particle size distribution is predicted from the selection and breakage matrices for $n = 38$ size classes. Then, the corresponding PGB is computed from the predicted particle size distribution. Finally, equation (26) provides the predicted flow function coefficient. It appears on Figure 14 that this methodology successfully predicts the flowability of the powder after 16 minutes of grinding. This is all the more interesting considering that the selection and breakage parameters, did not have to be computed again to make this prediction. This confirms the assumption stating that these parameters are not a function of time for the case studied. Likewise, the power law given by equation (26) seems to provide valid predictions for 16 minutes of grinding, despite the fact that its coefficients were found from measurements performed on samples ground for 0.4 to 8 minutes only. However, it should be noted that the flow function coefficient does not vary very much after 10 minutes of grinding, making such an extrapolation easier.

5. Conclusion and perspectives

In this paper, we showed that the population balance model could be used to predict the evolution of the particle size distribution of an alumina powder according to the time spent in a ball mill. In particular, Kapur's first order approximation was shown to be consistent with the experimental data for up to 8 minutes of grinding. The grinding kinetic model, which is usually applied for particle size distributions obtained by sieving was shown to be also suitable with particle size distributions measured by LASER diffraction despite the much finer size classes involved. This allowed estimating the selection and breakage function from a relatively small amount of grinding tests and characterizations. The PGB of the powder samples was then computable for any grinding time from the predicted particle size distributions. The results obtained highlighted the fact that this dimensionless number is highly dependent on the precision of the particle size distribution, especially for the fine particles area. Finally, the macro/micro power law correlation, represented by equation (3), linking the flow function coefficient to the PGB was shown to be very consistent with the experimental data.

The overall method allowed to predict efficiently the evolution of the flowability of the alumina powder investigated through the grinding process. In addition, the extrapolation of the model is still consistent after 16 minutes of grinding, despite the fact that the model parameters S_i , b_{ij} , α and β were established from experimental data collected during the first 8 minutes of grinding only. Such a verification shows that this methodology allows to predict the evolution of the flowability of a given ground powder according to the grinding time, from few samples taken at various grinding times and analyzed by LASER diffraction. Thus, this method may be used by industrials for estimating the processability of a powder after varying the grinding time.

In a previous study, we showed that the power law equation (3) could be used for predicting the flowability of co-ground powders prepared in a ball mill (Giraud et al., 2020b). This study suggested that such prediction was possible if the particle size distribution of all the

constituting powders, ground in exactly the same conditions, are known. However, this is not always possible in practice since mono-constituent grindings may not be realizable. The present paper opens a path to get rid of this constraint by computing the multi-component population-dependent granular Bond number of the co-ground samples directly from the particle size distributions of the constituent raw powders, knowing their selection and breakage functions. Such an approach should be tested in the future.

Finally, this work showed that the evolution of the flowability of the alumina powder could be described analytically as a function of the grinding time by combining equations (18), (24), (25) and (26). Thus, it would be interesting to investigate the influence of the parameters α_1 and α_2 , which depend on the particle breakage behavior and on the grinding conditions, on the evolution of the flow function coefficient through the grinding time. It should also be noted that a link between the flowability, measured by shear tests, and the selection and breakage function has been found. It is then tempting to investigate a reverse model allowing to assess the selection and breakage parameters from simple shear tests carried out after different grinding times. Such reverse model should be explored in future works.

Bibliography

- Arai, Y., 1996. *Chemistry of Powder Production*, Particle Technology Series. Springer Netherlands.
- Austin, L.G., 1971. Introduction to the mathematical description of grinding as a rate process. *Powder Technol.* 5, 1–17. [https://doi.org/10.1016/0032-5910\(71\)80064-5](https://doi.org/10.1016/0032-5910(71)80064-5)
- Austin, L.G., Bagga, P., 1981. An analysis of fine dry grinding in ball mills. *Powder Technol.* 28, 83–90. [https://doi.org/10.1016/0032-5910\(81\)87014-3](https://doi.org/10.1016/0032-5910(81)87014-3)
- Austin, L.G., Rogers, R.S.C., 1985. Powder technology in industrial size reduction. *Powder Technol.* 42, 91–109. [https://doi.org/10.1016/0032-5910\(85\)80041-3](https://doi.org/10.1016/0032-5910(85)80041-3)
- Beach, E.R., Tormoen, G.W., Drelich, J., Han, R., 2002. Pull-off Force Measurements between Rough Surfaces by Atomic Force Microscopy. *J. Colloid Interface Sci.* 247, 84–99. <https://doi.org/10.1006/jcis.2001.8126>
- Bernard-Granger, G., Giraud, M., Pascal, E., Mailhan, L., Larsson, T., Valot, C., Ablitzer, C., Gatamel, C., Berthiaux, H., 2019. Rheological properties of alumina powder mixtures investigated using shear tests. *Powder Technol.* 345, 300–310. <https://doi.org/10.1016/j.powtec.2019.01.027>
- Berthiaux, H., Dodds, J., 1999. Modelling fine grinding in a fluidized bed opposed jet mill: Part I: Batch grinding kinetics. *Powder Technol.* 106, 78–87. [https://doi.org/10.1016/S0032-5910\(99\)00049-2](https://doi.org/10.1016/S0032-5910(99)00049-2)
- Berthiaux, H., Dodds, J., 1997. A new estimation technique for the determination of breakage and selection parameters in batch grinding. *Powder Technol.* 94, 173–179. [https://doi.org/10.1016/S0032-5910\(97\)03323-8](https://doi.org/10.1016/S0032-5910(97)03323-8)
- Berthiaux, H., Varinot, C., Dodds, J., 1996. Approximate calculation of breakage parameters from batch grinding tests. *Chem. Eng. Sci.* 51, 4509–4516. [https://doi.org/10.1016/0009-2509\(96\)00275-8](https://doi.org/10.1016/0009-2509(96)00275-8)
- Capece, M., Ho, R., Strong, J., Gao, P., 2015. Prediction of powder flow performance using a multi-component granular Bond number. *Powder Technol.* 286, 561–571. <https://doi.org/10.1016/j.powtec.2015.08.031>
- Capece, M., Silva, K.R., Sunkara, D., Strong, J., Gao, P., 2016. On the relationship of inter-particle cohesiveness and bulk powder behavior: Flowability of pharmaceutical powders. *Int. J. Pharm.* 511, 178–189. <https://doi.org/10.1016/j.ijpharm.2016.06.059>
- Castellanos, A., 2005. The relationship between attractive interparticle forces and bulk behaviour in dry and uncharged fine powders. *Adv. Phys.* 54, 263–376. <https://doi.org/10.1080/17461390500402657>
- Chen, Y., Yang, J., Dave, R.N., Pfeffer, R., 2008. Fluidization of coated group C powders. *AIChE J.* 54, 104–121. <https://doi.org/10.1002/aic.11368>
- EFCE, 1989. Standard shear testing technique for particulate solids using the Jenike shear cell, EFCE Working Party on the Mechanics of Particulate. ed. Institution of Chemical Engineers.
- Fu, X., Huck, D., Makein, L., Armstrong, B., Willen, U., Freeman, T., 2012. Effect of particle shape and size on flow properties of lactose powders. *Adv. Charact. Model. Part. Process.* 10, 203–208. <https://doi.org/10.1016/j.partic.2011.11.003>
- Giraud, M., Gatamel, C., Vaudez, S., Bernard-Granger, G., Nos, J., Gervais, T., Berthiaux, H., 2020a. Investigation of a granular Bond number based rheological model for polydispersed particulate systems. Press.
- Giraud, M., Vaudez, S., Gatamel, C., Nos, J., Gervais, T., Bernard-Granger, G., Berthiaux, H., 2020b. Predicting the flowability of powder mixtures from single components properties through the multi-component population-dependent granular Bond number; extension to ground powder mixtures. *Powder Technol.*

- Gupta, V.K., 2017. Effect of size distribution of the particulate material on the specific breakage rate of particles in dry ball milling. *Powder Technol.* 305, 714–722. <https://doi.org/10.1016/j.powtec.2016.10.075>
- Israelachvili, J.N., 2011. Chapter 13 - Van der Waals Forces between Particles and Surfaces, in: *Intermolecular and Surface Forces (Third Edition)*. Academic Press, San Diego, pp. 253–289. <https://doi.org/10.1016/B978-0-12-375182-9.10013-2>
- Kapur, P.C., 1971. *Minerals Beneficiation - Kinetics of Batch Grinding-Part B: An Approximate Solution to the Grinding Equation*. The American Institute of Mining, Metallurgical, and Petroleum Engineers.
- Leturia, M., Benali, M., Lagarde, S., Ronga, I., Saleh, K., 2014. Characterization of flow properties of cohesive powders: A comparative study of traditional and new testing methods. *Powder Technol.* 253, 406–423. <https://doi.org/10.1016/j.powtec.2013.11.045>
- Liu, L.X., Marziano, I., Bentham, A.C., Litster, J.D., E.T.White, Howes, T., 2008. Effect of particle properties on the flowability of ibuprofen powders. *Int. J. Pharm.* 362, 109–117. <https://doi.org/10.1016/j.ijpharm.2008.06.023>
- Mellmann, J., 2001. The transverse motion of solids in rotating cylinders—forms of motion and transition behavior. *Powder Technol.* 118, 251–270. [https://doi.org/10.1016/S0032-5910\(00\)00402-2](https://doi.org/10.1016/S0032-5910(00)00402-2)
- Mellmann, J., Hoffmann, T., Fürll, C., 2013. Flow properties of crushed grains as a function of the particle shape. *Powder Technol.* 249, 269–273. <https://doi.org/10.1016/j.powtec.2013.06.035>
- Molerus, O., 1982. Interpretation of Geldart's type A, B, C and D powders by taking into account interparticle cohesion forces. *Powder Technol.* 33, 81–87. [https://doi.org/10.1016/0032-5910\(82\)85041-9](https://doi.org/10.1016/0032-5910(82)85041-9)
- Petrakis, E., Stamboliadis, E., Komnitsas, K., 2017. Identification of Optimal Mill Operating Parameters during Grinding of Quartz with the Use of Population Balance Modeling. *KONA Powder Part. J.* 34, 213–223. <https://doi.org/10.14356/kona.2017007>
- Prasher, C.L., 1987. *Crushing and grinding process handbook*. Wiley.
- Reid, K.J., 1965. A solution to the batch grinding equation. *Chem. Eng. Sci.* 20, 953–963. [https://doi.org/10.1016/0009-2509\(65\)80093-8](https://doi.org/10.1016/0009-2509(65)80093-8)
- Rumpf, H., 2012. *Particle Technology, Particle Technology Series*. Springer Netherlands.
- Schulze, D., 2007. *Powders and Bulk Solids: Behavior, Characterization, Storage and Flow*. Springer Berlin Heidelberg.
- Seville, J.P., Tüzün, U., Clift, R., 2012. *Processing of Particulate Solids, Particle Technology Series*. Springer Netherlands.
- Seville, J.P.K., Willett, C.D., Knight, P.C., 2000a. Interparticle Forces in Fluidisation: A Review. *Powder Technol.* 113, 261–268.
- Seville, J.P.K., Willett, C.D., Knight, P.C., 2000b. Interparticle forces in fluidisation: a review. *Neptis Symp. Fluid.- Present Future* 113, 261–268. [https://doi.org/10.1016/S0032-5910\(00\)00309-0](https://doi.org/10.1016/S0032-5910(00)00309-0)
- Shoji, K., Austin, L.G., Smaila, F., Brame, K., Luckie, P.T., 1982. Further studies of ball and powder filling effects in ball milling. *Powder Technol.* 31, 121–126. [https://doi.org/10.1016/0032-5910\(82\)80013-2](https://doi.org/10.1016/0032-5910(82)80013-2)
- Tisserand, C., Calvet, R., Patry, S., Galet, L., Dodds, J.A., 2009. Comparison of two techniques for the surface analysis of alumina (Al₂O₃): Inverse Gas Chromatography at Finite Concentration (IGC-FC) and Dynamic Vapor Sorption (DVS). *Powder Technol.* 190, 53–58. <https://doi.org/10.1016/j.powtec.2008.04.058>

List of figures:

Graphical abstract

Figure 1: Representation experimental setup used for grinding the powders. The powder and the pebbles are contained in the cylindrical vessel, rotating around its longitudinal axis.

Figure 2: Volume particle size distribution of the alumina GE15 powder before and after various grinding tests.

Figure 3: Schematic representation of the methodology employed in order to predict the flowability of the ground powder according to the grinding time.

Figure 4: Schematic representation of the width of the particle size classes, represented as a geometric progression by rectangles, for the initial particle size distribution and for configurations with 38 and 8 size classes.

Figure 5: Cumulative oversize particle size distribution of the alumina powder after six minutes of grinding, represented over 8 (a) or 38 (b) size classes.

Figure 6: Representation of Kapur's first order approximation (dotted lines) for each size classes ($n=8$). The experimental data are represented by the squares, triangles, rounds and diamonds.

Figure 7: Evolution of the selection parameters as a function of the particle size.

Figure 8: Cumulative breakage parameters represented for each size class ($n=8$) as a function of the relative size. Class 7 and 8 are not represented sin particle fragmentation do not take place in those classes (the corresponding parameters the B matrix are zeros).

Figure 9: Comparison between measured and predicted particle size distributions of the alumina powder after 6 minutes of grinding ($n=8$).

Figure 10: Evolution of the mean Sauter diameter calculated from the particle size distributions measured by LASER diffraction (points) and predicted by the model (crosses) for $n=8$ and $n=38$.

Figure 11: Total squared error obtained between the measured and predicted particle size distributions after various grinding durations for $n=8$ of $n=38$.

Figure 12: Evolution of the population-dependent granular Bond number according to the grinding time, computed from measurements and from predictions made with $n=8$ or $n=38$.

Figure 13: Flow function coefficient of the alumina powder after different grinding durations, as a function of the population dependent granular Bond number represented on a logarithmic scale. The cross symbols correspond to experimental measurements, the continuous line corresponds to the power law those coefficients have been fitted with (26) and the dotted line corresponds to the law given by equation (4).

Figure 14: Evolution of the flow function coefficient of the alumina powder according to the grinding time. The experimental data are represented by the cross symbols and the model predictions, computed from the initial properties of the raw powders are represented by the continuous line and the squares. The residuals are represented on the top right corner.

Graphical abstract:

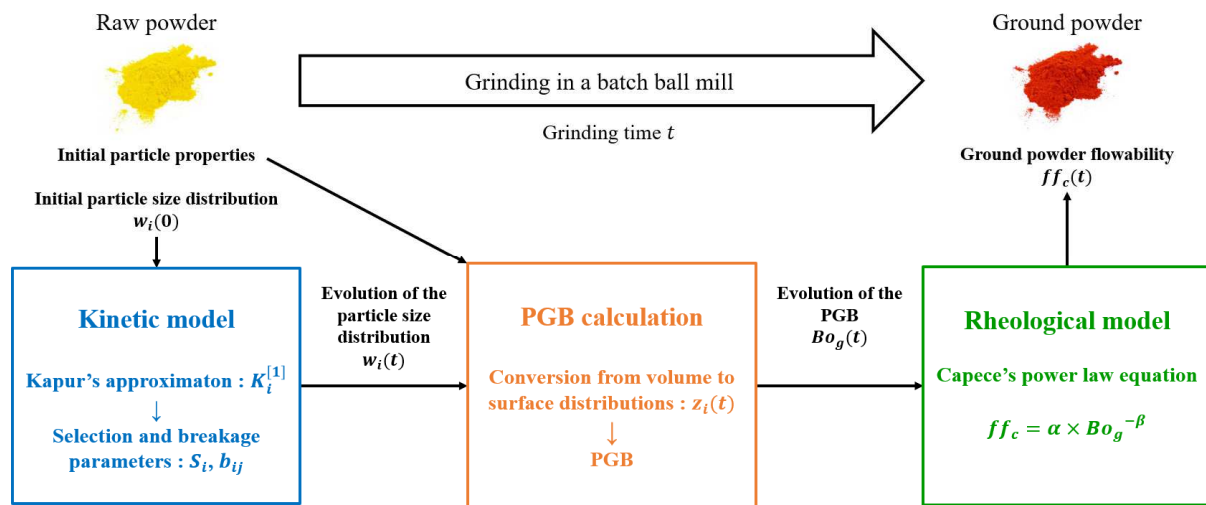


Figure 1:

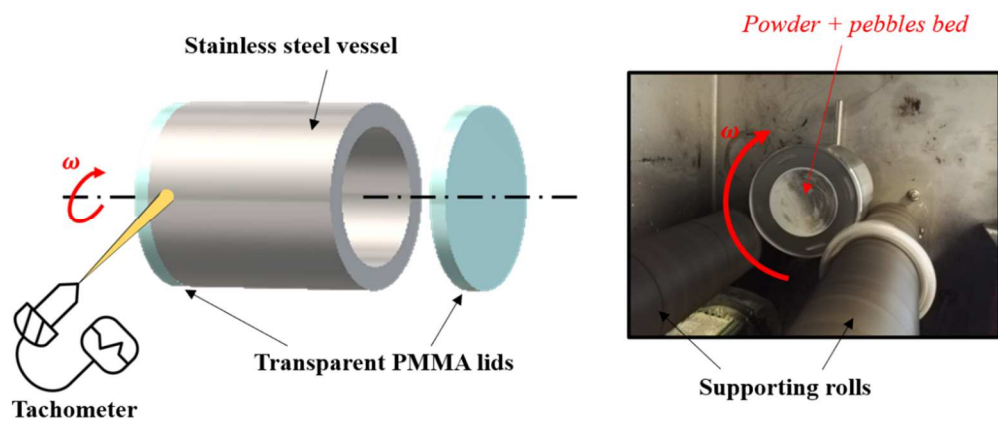


Figure 2:

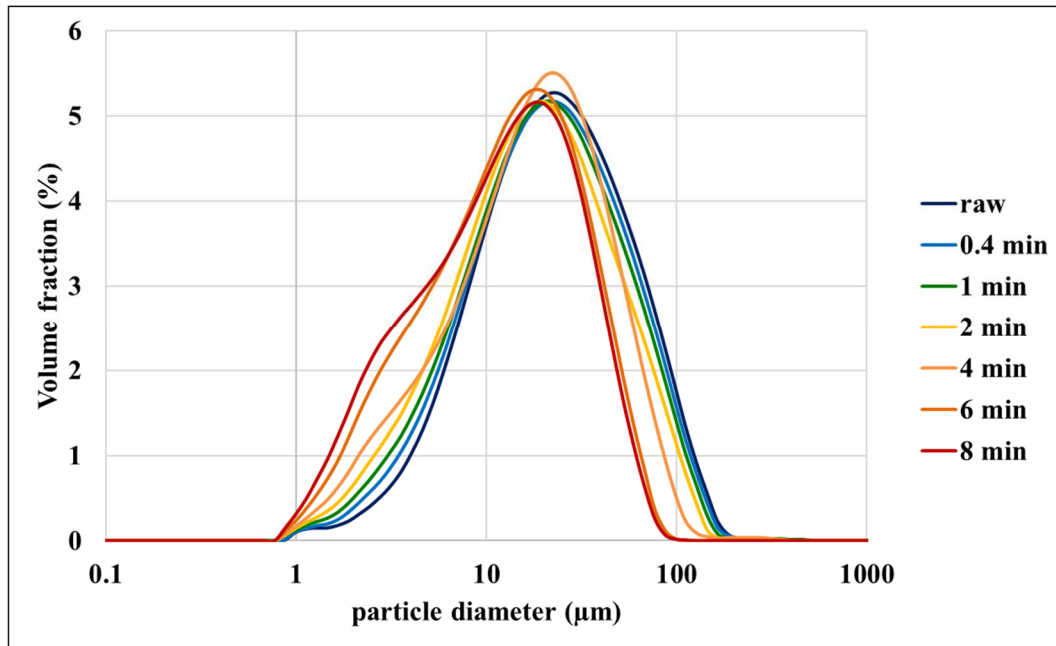


Figure 3:

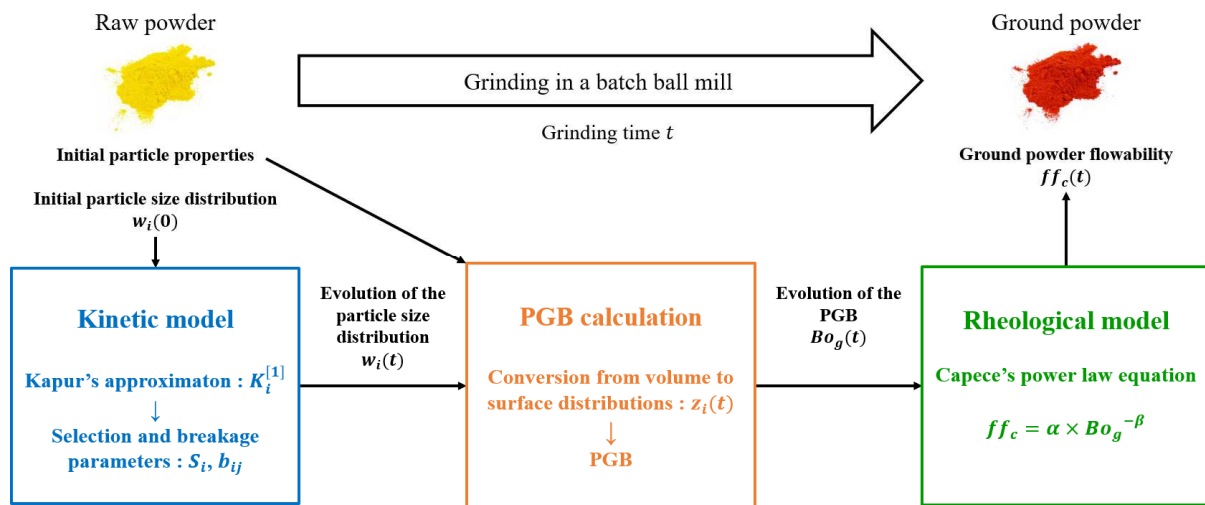


Figure 4:

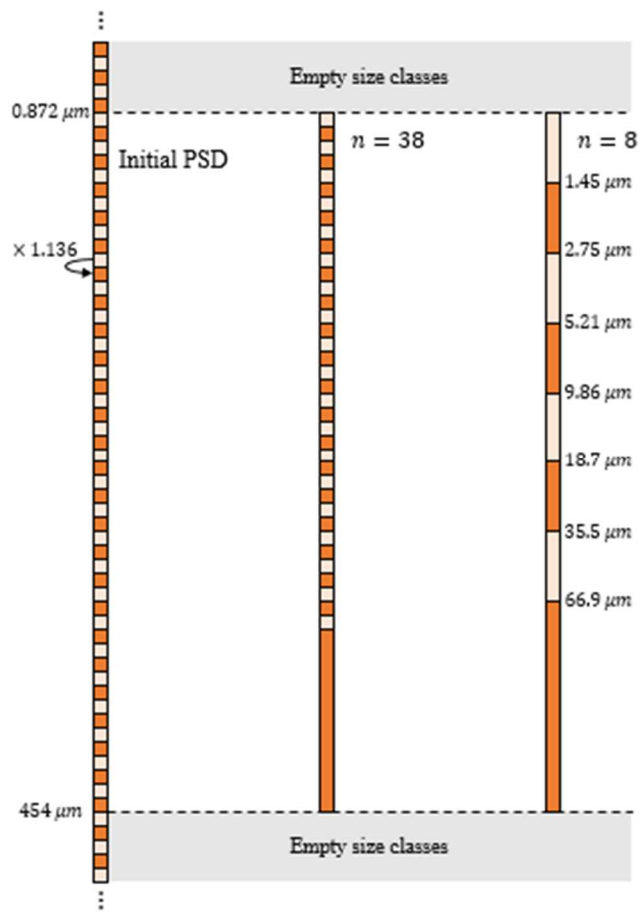


Figure 5:

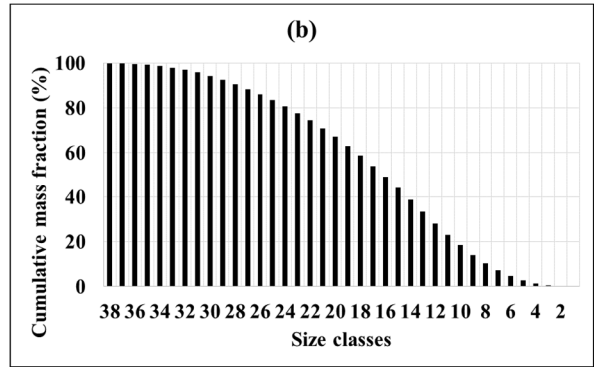
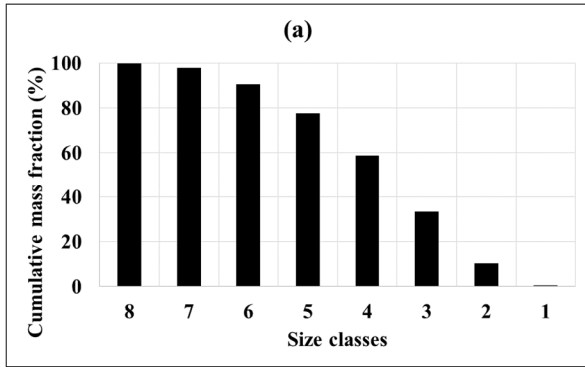


Figure 6:

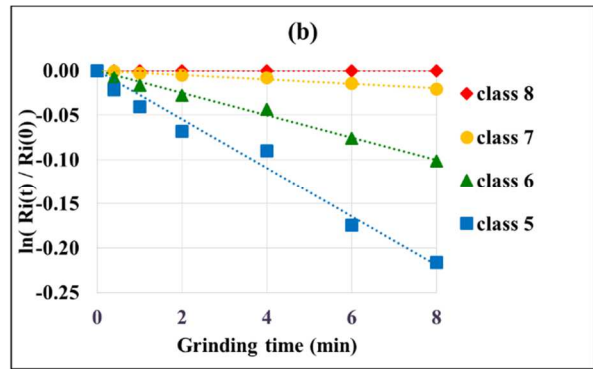
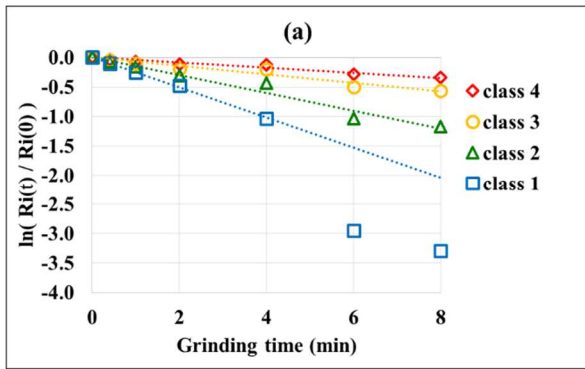


Figure 7:

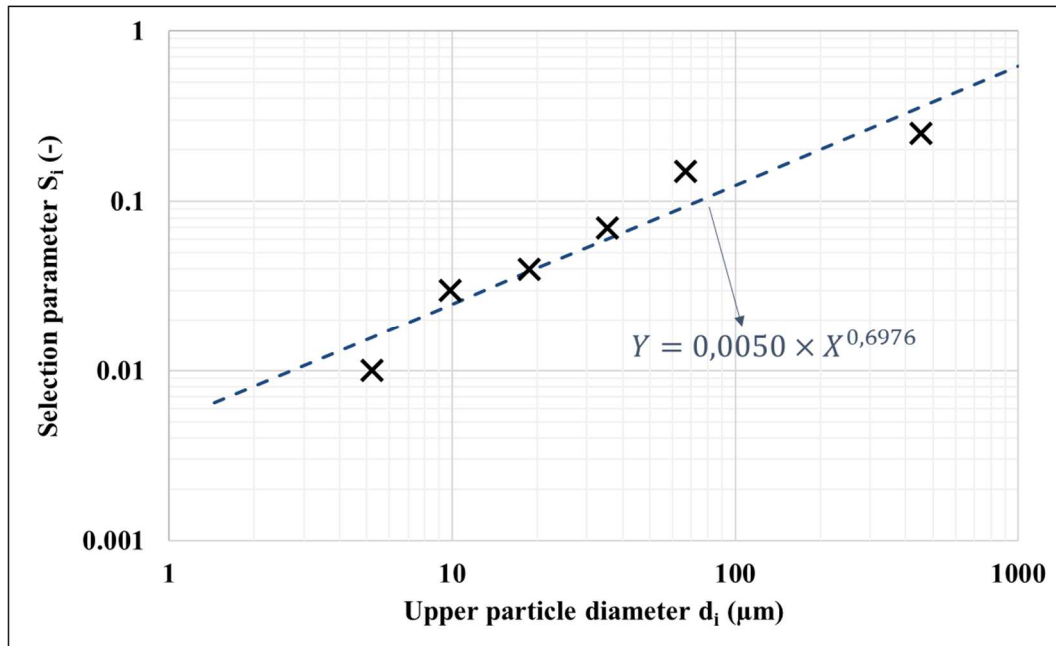


Figure 8:

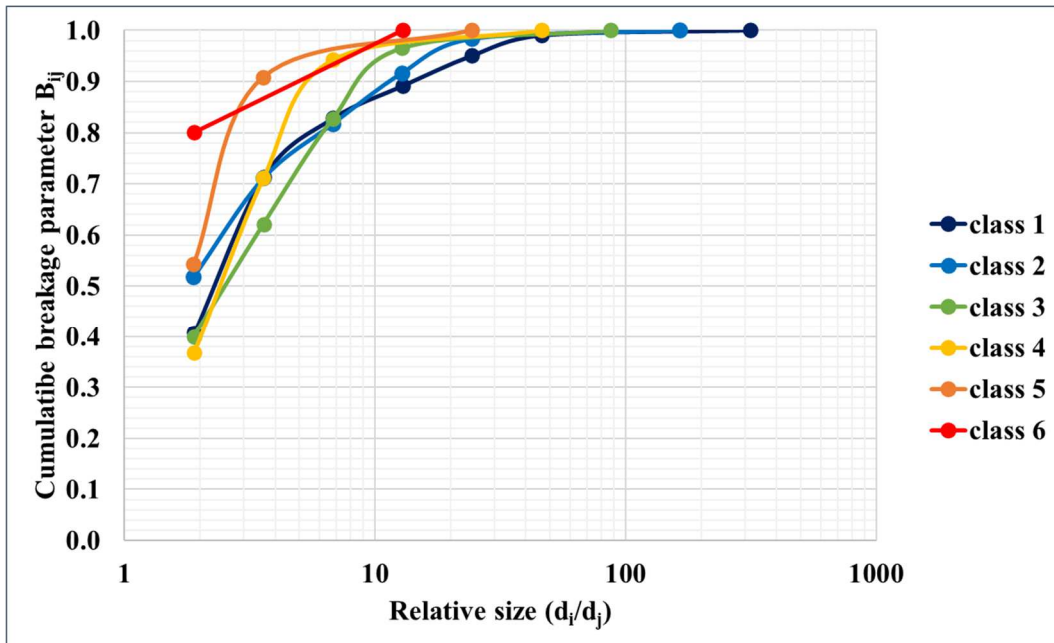


Figure 9:

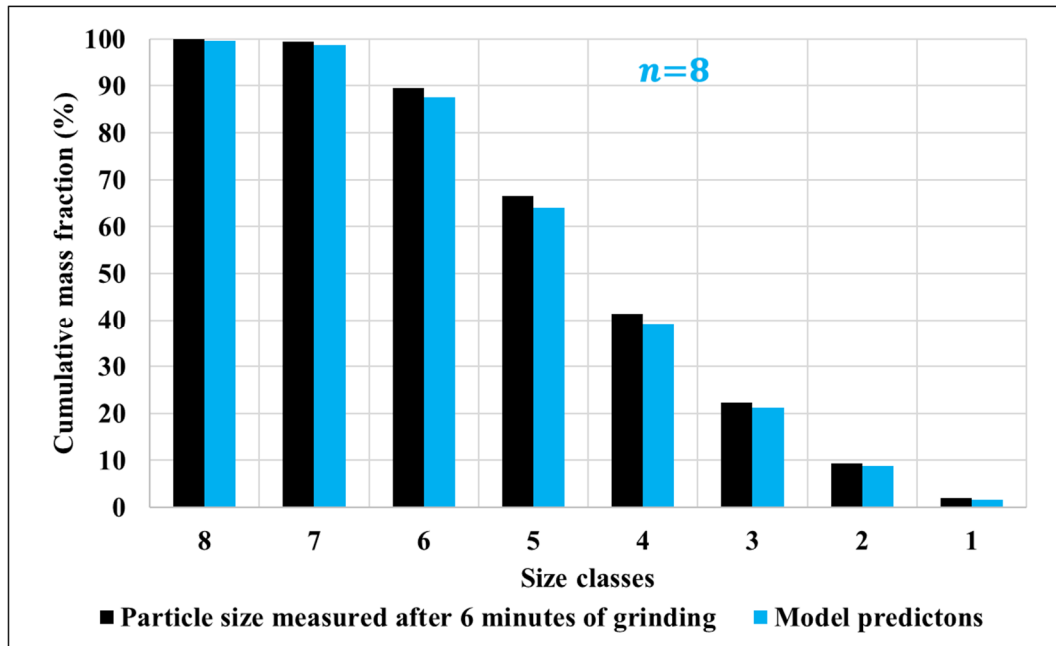


Figure 10:

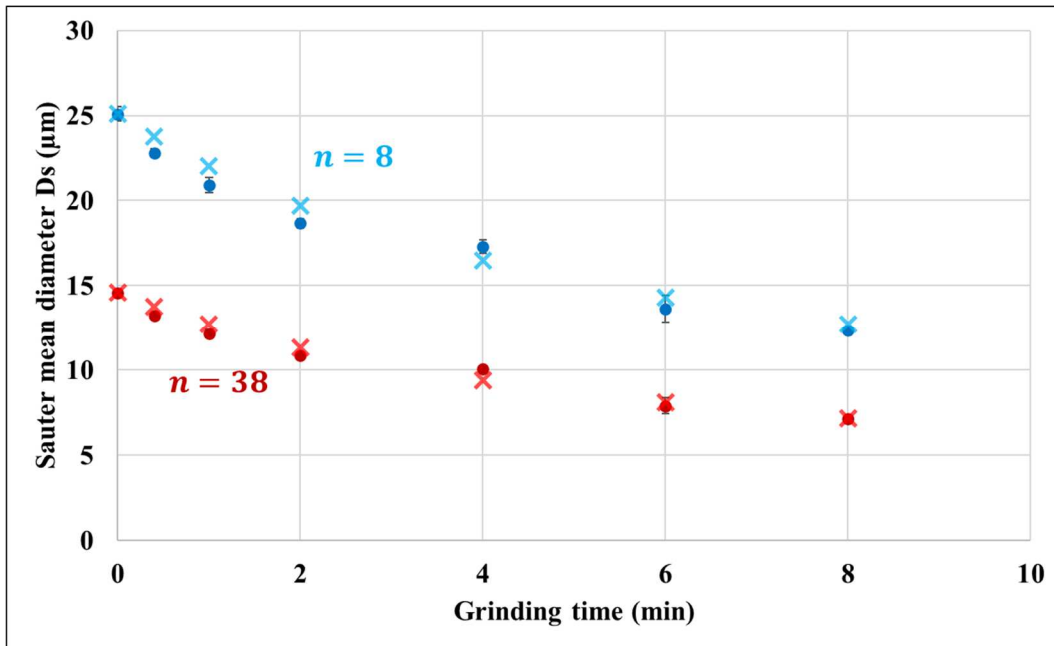


Figure 11:

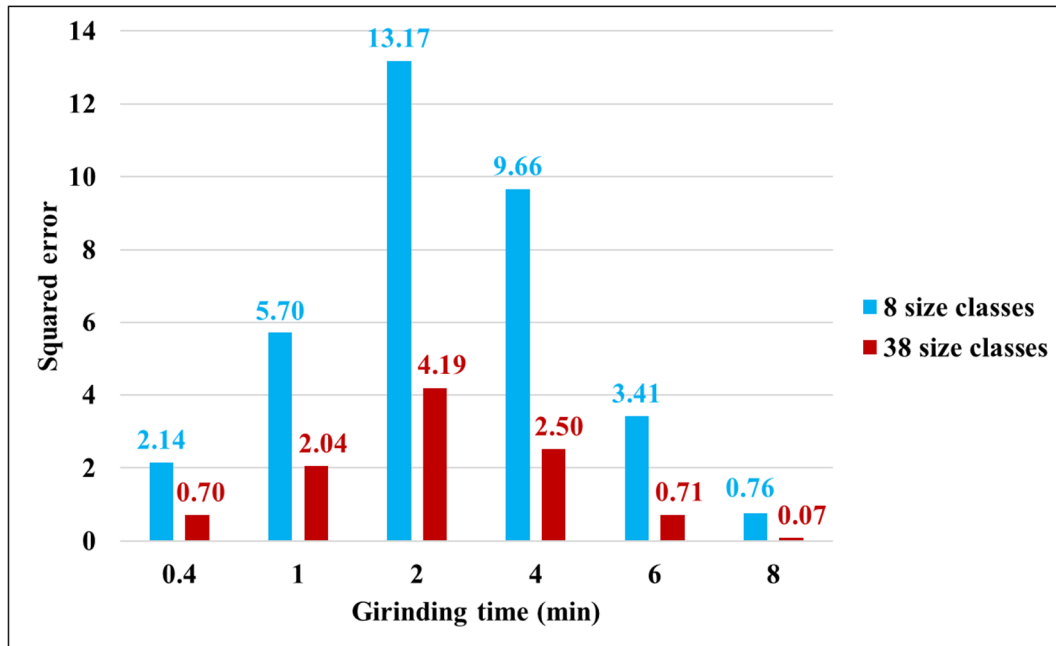


Figure 12:

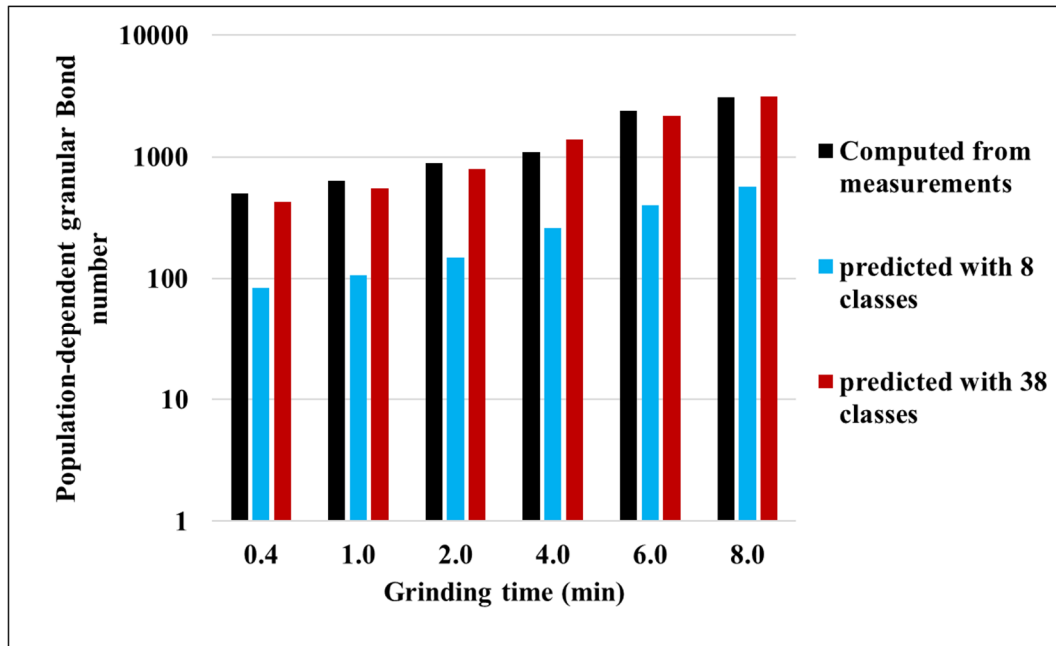


Figure 13:

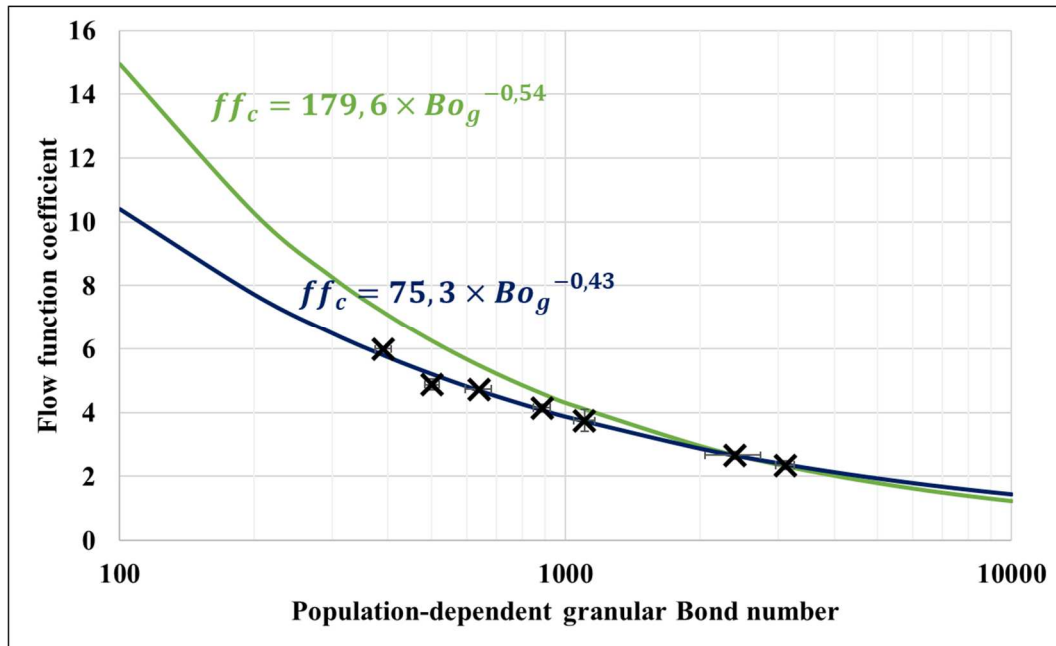
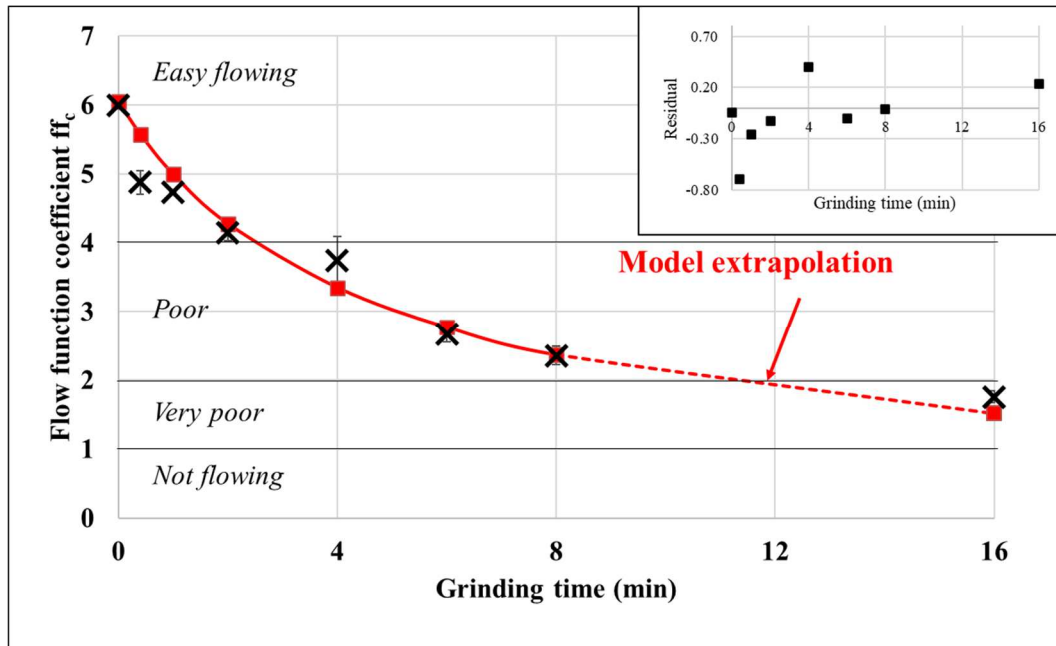


Figure 14:



List of tables:

Table 1: Classification of the flowability of a given powder according to its flow function coefficient.

Table 2: Flow function coefficient, Sauter mean diameter and the corresponding population-dependent granular Bond number of the alumina GE15 powder after different grinding times.

Table 3: Kapur's first order coefficients, $K_i^{[1]}$, obtained from Figure 6, and the total squared error, ϵ_i corresponding to this approximation. The particle size distribution being defined over 8 size classes. The coefficients are computed after 8 minutes of grinding except for the first class for which Kapur's approximation seems to hold until 4 minutes of grinding only.

Table 4: Evolution of the population dependent granular Bond number according to the grinding time. Comparison between the Bond numbers computed from particles size distributions measured experimentally (Bo_g^{exp}), predicted for $n=38$ ($Bo_g^{n=38}$) and for $n=8$ ($Bo_g^{n=8}$).

Table 1:

Flow index value	Flowability
$ff_c < 1$	Not flowing
$1 < ff_c < 2$	Very poor
$2 < ff_c < 4$	Poor
$4 < ff_c < 10$	Easy
$ff_c > 10$	Free flowing

Table 2:

Grinding time (min)	Flow function coefficient ff_c (-)	Sauter mean diameter D_s (μm)	Population-dependent granular Bond number Bo_g (-)
Raw powder	5.99 ± 0.00	14.5 ± 0.24	391 ± 16
0.4	4.87 ± 0.17	13.2 ± 0.14	502 ± 19
1	4.73 ± 0.01	12.1 ± 0.25	638 ± 42
2	4.15 ± 0.12	10.8 ± 0.15	886 ± 38
4	3.75 ± 0.34	10.0 ± 0.24	1103 ± 58
6	2.67 ± 0.11	7.9 ± 0.46	2395 ± 345
8	2.35 ± 0.14	7.1 ± 0.10	3105 ± 145

Table 3:

Class number i	$K_i^{[1]}$	ϵ_i	Class number i	$K_i^{[1]}$	ϵ_i
1 (4 min)	-0.2533	0.0014	5	-0.0274	0.0009
2	-0.1501	0.0461	6	-0.0125	0.0001
3	-0.0725	0.0157	7	-0.0025	0.0000
4	-0.0435	0.0049	8	-0.0000	0.0000

Table 4:

Grinding time	Bo_g^{exp}	$Bo_g^{n=38}$	$Bo_g^{n=8}$
No grinding	391 ± 16	353	71
24 seconds	502 ± 19	427	84
1 minute	638 ± 42	551	106
2 minutes	886 ± 38	790	149
4 minutes	1103 ± 58	1394	258
6 minutes	2395 ± 345	2172	399
8 minutes	3105 ± 145	3134	571